Available online at www.sciencedirect.com
SCIENCE DIRECT
Journal of Molecular Catalysis A: Chemical 249 (2006) 135–142
JOURNAL OF MOLECULAR CATALYSIS A: CHEMICAL
www.elsevier.com/locate/molcata

Effects of calcination temperature on the microstructures and photocatalytic activity of titanate nanotubes

Jiaguo Yu [a,*], Huogen Yu [a], Bei Cheng [a], C. Trapalis [b]

[a] *State Key Laboratory of Advanced Technology for Material Synthesis and Processing, Wuhan University of Technology, Luoshi Road 122#, Wuhan 430070, PR China*
[b] *Institute of Materials Science, National Centre for Scientific Research "Demokritos" 153 10, Ag. Paraskevi, Attikis, Greece*

Received 26 November 2005; received in revised form 22 December 2005; accepted 4 January 2006
Available online 10 February 2006

Abstract

Titanate nanotubes were prepared via a hydrothermal treatment of TiO_2 powders (P25) in a 10 M NaOH solution at 150 °C for 48 h and then calcined at various temperatures. The as-prepared titanate nanotubes before and after calcination were characterized with XRD, TEM, HRTEM, SEM, FESEM, and nitrogen adsorption–desorption isotherms. The photocatalytic activity of the as-prepared samples was evaluated by photocatalytic oxidation of acetone in air. The effects of calcination temperature on the phase structure, crystallite size, morphology, specific surface area, pore structures and photocatalytic activity of the titanate nanotubes were investigated. The results indicated that at 400 to 600 °C, the calcined nanotube samples showed a higher photocatalytic activity than Degussa P25. Especially, at 400 and 500 °C, the photocatalytic activity of the calcined nanotubes exceeded that of P25 by a factor of about 3.0 times. This could be attributed to the fact that the former had a larger specific surface area and pore volume. With further increase in the calcination temperature from 700 to 900 °C, the photocatalytic activity of the calcined nanotube samples greatly decreased due to the formation of rutile phase, the sintering and growth of TiO_2 crystallites and the decrease of specific surface area and pore volume.

Keywords: Calcination; TiO_2; Titanate nanotubes; Microstructures; Photocatalytic activity

1. Introduction

Many efforts have been focused on the semiconductor photocatalysts for their environmental applications in air purification, water disinfection, and hazardous water remediation since Honda and Fujishima discovered the photocatalytic splitting of water on the TiO_2 electrodes in 1972 [1–9]. Among various oxide semiconductor photocatalysts, titania is a very important photocatalyst due to its biological and chemical inertness, strong oxidizing power, nontoxicity and long-term stability against photo and chemical corrosion [1–9]. Despite its great potential, the low photocatalytic efficiency of TiO_2 hinders the commercialization of photocatalytic oxidation technology [10]. Therefore, the further improvement of photoactivity of TiO_2 is one of the most important tasks from the point of view of practical use. To achieve this purpose, it is of great interest to develop TiO_2 photocatalyst with highly photocatalytic activity.

Recently, TiO_2 and/or titanate nanotubes with large specific surface area and pore volume have appeared to be a promising and important prospect due to their fascinating microstructures and promising photo-electrochemical applications since the innovative work was reported by Kasuga et al. [11–19]. Using a simple hydrothermal treatment of crystalline TiO_2 particles with NaOH aqueous solutions, high-quality nanotubes with uniform diameter of around 10 nm were obtained and their specific surface area reached more than 400.0 m^2/g [11,12]. By optimizing the preparation conditions, such as the hydrothermal treatment time and temperature, high-yield nanotubes could be effectively prepared by this simple, cost-effective, and environmentally friendly technology [20]. Moreover, several studies indicated that TiO_2 nanotubes possessed better properties in photocatalysis [21,22] and sensing [23], in comparison to colloidal or other forms of TiO_2. Unfortunately, the nanotubes prepared by this hydrothermal method showed almost no photocatalytic activity for the photocatalytic degradation of acetone in our

* Corresponding author. Tel.: +86 27 8788 3610; fax: +86 27 8788 3610.
E-mail address: jiaguoyu@yahoo.com (J. Yu).

1381-1169/$ – see front matter © 2006 Elsevier B.V. All rights reserved.
doi:10.1016/j.molcata.2006.01.003

experiment. Following the pioneering works, the obtained nanotubes were actually not TiO_2, but might be hydrogen titanate [14,24]. Considering their large specific surface area, high pore volume, and unique morphology, the obtained nanotubes will offer another possibility to design various TiO_2-related materials by post-treatment methods, such as hydrothermal post-treatment and well-controlled calcination. Moreover, it is an important issue to study the structure stability of the nanotubes and their corresponding crystalline phase at various calcination temperatures from the point of view of practical use of titanate nanotubes.

In the present work, titanate nanotubes were first prepared by a hydrothermal reaction using a 10 M NaOH aqueous solution and Degussa P25 as precursors. Subsequently, the as-prepared nanotubes were washed and then calcined at various temperatures. The photocatalytic activity of the titanate nanotubes before and after calcination was evaluated by photocatalytic oxidation of acetone in air. The effects of calcination temperature on the phase structure, crystallite size, morphology, specific surface area, pore structures and photocatalytic activity of the titanate nanotubes were investigated.

2. Experimental

2.1. Preparation of titanate nanotubes

Titanate nanotubes were prepared using a chemical process similar to that described by Kasuga et al. [11,12]. TiO_2 source used for the titanate nanotubes was commercial-grade TiO_2 powder (P25, Degussa AG, Germany) with crystalline structure of ca. 20% rutile and ca. 80% anatase and primary particle size of ca. 30 nm. In a typical preparation, 1.5 g of the TiO_2 powder (P25) was mixed with 140 ml of 10 M NaOH solution followed by hydrothermal treatment of the mixture at 150 °C in a 200 ml Teflon-lined autoclave for 48 h. After hydrothermal reaction, the precipitate was separated by filtration and washed with a 0.1 M HCl solution and distilled water until the pH value of the rinsing solution reached ca. 6.5, approaching the pH value of the distilled water. The washed samples were dried in a vacuum oven at 80 °C for 8 h and then calcined at 300, 400, 500, 600, 700, 800 and 900 °C in air for 2 h, respectively.

2.2. Characterization

X-ray diffraction (XRD) patterns were obtained on a D/MAX-RB X-ray diffractometer (Rigaku, Japan) using Cu Kα irradiation at a scan rate (2θ) of 0.05° s^{-1} and were used to determine the identity of any phase present and their crystallite size. The accelerating voltage and the applied current were 15 kV and 20 mA, respectively. Transmission electron microscopy (TEM) analyses were conducted with a JEM-2010FEF electron microscope (JEOL, Japan), using 200 kV accelerating voltage. Morphology observation was performed on a JSM-6700F field emission scanning electron microscope (FESEM, JEOL, Japan) and a JSM-5610LV scanning electron microscope (SEM, JEOL, Japan). Nitrogen adsorption–desorption isotherms were obtained on an ASAP 2020 (Micromeritics Instruments, USA) nitrogen adsorption apparatus. All the samples were degassed at 100 °C prior to BET measurements. The Brunauer–Emmett–Teller (BET) specific surface area (S_{BET}) was determined by a multipoint BET method using the adsorption data in the relative pressure (P/P_0) range of 0.05–0.25. Desorption isotherm was used to determine the pore size distribution using the Barret–Joyner–Halender (BJH) method [25]. The nitrogen adsorption volume at the relative pressure (P/P_0) of 0.970 was used to determine the pore volume and the average pore size.

2.3. Measurement of photocatalytic activity

Acetone (CH_3COCH_3) is a common chemical that is used extensively in the industrial and domestic fields. Therefore, we chose it as a model contaminate chemical. Photocatalytic oxidation of acetone is based on the following reaction [26–29]:

$$CH_3COCH_3 + 4O_2 \rightarrow 3CO_2 + 3H_2O \quad (1)$$

The measurement of photocatalytic activity of the titanate nanotubes before and after calcination was performed in a 15 L reaction reactor using the photodegradation of acetone with an initial concentration of 350 ± 20 ppm. The powder catalysts were prepared by coating an aqueous suspension of powder samples onto three dishes with a diameter of ca. 7.0 cm. The dishes containing catalysts were dried at 100 °C and then cooled to room temperature before being used. The weight of the catalysts used for each experiment was kept at ca. 0.5 g. After the catalysts were placed in the reactor, a small amount of acetone was injected with a syringe into the reactor. The reactor was connected to a $CaCl_2$-containing dryer used for controlling the initial humidity in the reactor. The acetone vapor was allowed to reach adsorption–desorption equilibrium with catalysts in the reactor prior to UV light irradiation. Integrated UV intensity in the range of 310–400 nm striking the coatings, measured with a UV radiometer (Model: UV-A, made in Photoelectric Instrument Factory of Beijing Normal University), was 2.5 mW/cm^2, while the peak wavelength of UV light was 365 nm. The concentration analysis of acetone, carbon dioxide and water vapor in the reactor was conducted on line with a Photoacoustic IR Multigas Monitor (INNOVA Air Tech Instruments Model 1312). The photocatalytic activity of the catalyst samples can be quantitatively evaluated by comparing the apparent reaction rate constants. The photocatalytic oxidation of acetone is a pseudo-first-order reaction and its kinetics may be expressed as follows: $\ln(C_0/C) = kt$ [27,28], where k is the apparent reaction rate constant, C_0 and C are the initial concentration and the reaction concentration of acetone, respectively.

3. Results and discussion

3.1. Morphology and structure of titanate nanotubes

Fig. 1a shows TEM image of titanate nanotubes obtained by a hydrothermal reaction using Degussa P25 and 10 M NaOH aqueous solution as precursors at 150 °C for 48 h. A large amount of nanotubes with a diameter of 7–15 nm and a length of several

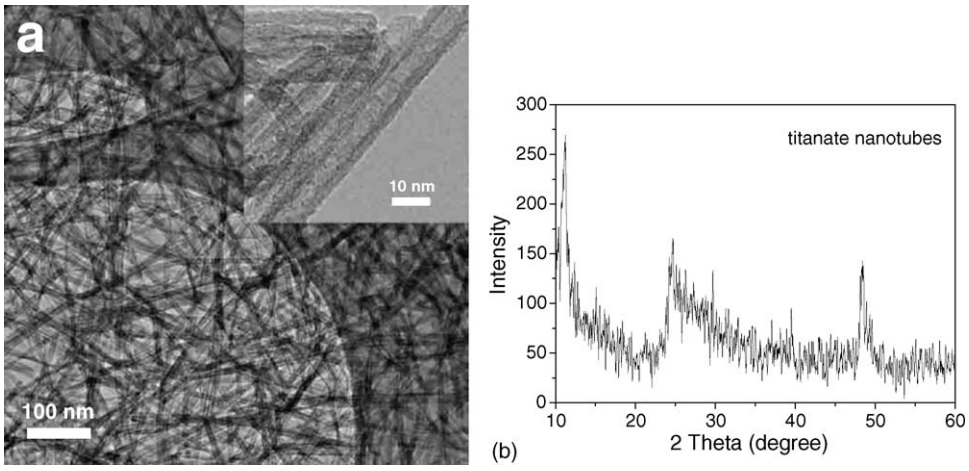

Fig. 1. TEM image and XRD pattern of the as-prepared titanate nanotubes.

hundreds nanometers were obtained. HRTEM image (inset in Fig. 1a) indicated that the prepared nanotubes possessed uniform inner and outer diameters along their length. Further observation indicated that the nanotubes were multi-layered and open-ended, in good agreement with the previous reports [13–15]. Fig. 1b shows the corresponding XRD pattern of the obtained nanotubes. After hydrothermal treatment of P25 in a 10 M NaOH solution for 48 h, the XRD pattern of the resulted powder (nanotubes) could not correspond to anatase, rutile, brookite or their mixtures. The crystal structure of the nanotubes was similar to that of $H_2Ti_3O_7$ ($Na_2Ti_3O_7$) [13,14], $Na_xH_{2-x}Ti_3O_7$ [24], $H_xTi_{2-x/4}\square_{x/4}O_4$ ($x = 0.75$) [30], probably due to their same layered titanate family. EDX analysis clearly demonstrated the absence of sodium ions in the obtained nanotubes. Therefore, the obtained nanotubes can be attributed to the hydrogen titanate.

3.2. Effects of calcination temperature on the microstructures and morphology of the titanate nanotubes

XRD was used to investigate the changes of phase structure and crystallite size of the nanotubes before and after calcination at different temperatures. Fig. 2 shows the XRD patterns of the titanate nanotubes calcined at various temperatures. It can be seen that all the diffraction peaks of the samples calcined at 300–600 °C can be indexed with the anatase phase of TiO_2. In the previous studies, different phase structures were obtained after the calcination of titanate nanotubes. On one hand, Suzuki and Yoshikawa [31] demonstrated the formation of TiO_2 (B) phase (a metastable polymorph of titanoium dioxide) after calcination and no anatase phase was found. On the other hand, Bruce and co-workers [32] reported that after calcination at 400–600 °C, layered hydrogen titanates nanowires were converted to the titanium dioxide polymorph TiO_2-B, while layered hydrogen titanates nanotubes were transformed to anatase with the loss of the tubular morphology. Many other researchers [24,30,33] also found that only anatase phase was formed after the calcination of hydrogen titanate nanotubes, in good agreement with our present results. The difference in the phase structure of the calcined nanotubes may be attributed to different preparation and post-treatment conditions. With increasing calcination temperature from 300 to 600 °C, the peak intensities of anatase increased significantly, indicating the improvement of crystallization of anatase phase. Simultaneously, the width of the (1 0 1) peak became narrower, suggesting the growth of anatase crystallites. At 700 °C, the diffraction peaks of both anatase and rutile phases were present in the calcined samples. This indicated that the phase transformation temperature of anatase to rutile was ca. 700 °C. Tsai and Teng [33] found that the onset temperature for the anatase-to-rutile phase transformation varied with the synthesis temperature of nanotube, and the phase transformation temperature of anatase to rutile was ca. 900 °C when the synthesis temperature of nanotubes was 150 °C. Though the present phase transformation temperature (700 °C) was lower than the above result (900 °C), it was in good agreement with that of pure TiO_2 samples. Usually, for pure TiO_2 samples, the rutile phase starts to appear at ca. 700 °C [5]. When the calcination temperature reached 800 °C, only rutile phase was found in the XRD pattern, indicating a narrow temperature range of phase transformation from anatase to rutile. It has been reported that

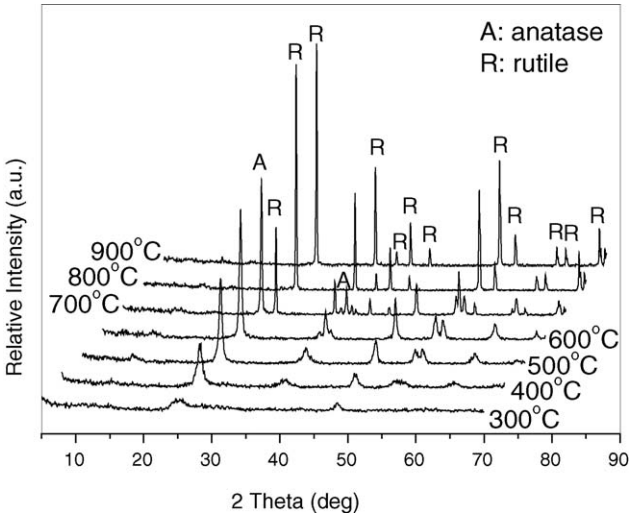

Fig. 2. XRD patterns of the titanate nanotubes calcined at various temperatures.

Table 1
Effects of calcination temperature on phase structure and average crystallite size (nm) of titanate nanotubes[a]

	Nanotubes	300 °C	400 °C	500 °C	600 °C	700 °C	800 °C	900 °C
D_A	0	5.3	11.6	18.34	28.7	41.3	0	0
D_R	0	0	0	0	0	62.5	>200	>200

[a] D_A and D_R denote the average crystallite size of anatase and rutile in the calcined titanate samples, respectively.

the phase transformation temperature and the temperature range of phase transformation mainly depend on the particle sizes, morphologies of crystals, and the addition of additives [34]. In this study, the narrow temperature range of phase transformation from anatase to rutile (ca. 700–800 °C) may be attributed to the formation of pure TiO_2 phase due to the dehydration of hydrogen titanate [35]. The average crystallite size of the calcined nanotube samples calculated using Scherrer's equation for the main diffraction peak, is presented in Table 1. With increasing calcination temperature from 300 to 600 °C, the crystallite size of anatase increased from 5.3 to 28.7 nm. At 700 °C, rutile began to form, resulting in an obvious increase in crystallite size. When the calcination temperature was over 700 °C, the crystallite size of rutile reached over 200 nm due to the phase transformation from antase to rutile and the sintering and growth of rutile.

The nitrogen adsorption–desorption isotherms of the titanate nanotubes before and after calcination are presented in Fig. 3. It can be seen that all the samples show a type H3 hysteresis loop according to BDDT classification [25], indicating the presence of mesopores (2–50 nm). Moreover, as for the titanate nanotubes calcined at a temperature lower than 800 °C, the observed hysteresis loops approach $P/P_0 = 1$, suggesting the presence of macropores (>50 nm) [36]. On the other hand, with increasing calcination temperature, the hysteresis loops shift to the region of higher relative pressure and the areas of the hysteresis loops gradually become small. When the calcination temperature was higher than 700 °C, the hysteresis loops of the samples were difficult to be observed.

Fig. 4 shows the corresponding pore size distributions of the titanate nanotubes before and after calcination at various temperatures. It can be seen that the pore size distributions of the titanate nanotubes strongly depend on the calcination temperature. Prior to calcination, the nanotubes exhibit a wide pore size distribution ranging from 1.5 to more than 100 nm. This was in good agreement with the previous studies, though different TiO_2 sources were used as the precursors [33,36]. Considering the morphology of the nanotubes observed in Fig. 1a, the smaller pores (<10 nm) may correspond to the pores inside the nanotubes and the diameters of these pores are equal to the inner diameter of the nanotubes, while the larger pores (10–100 nm) can be attributed to the aggregation of the nanotubes [36]. With increasing calcination temperature, the pore size distribution of the nanotubes gradually becomes narrower. At 500 °C, the smaller pores (<10 nm) disappeared due to the collapse of the tube structure in the nanotubes during calcination (Fig. 4). With further increase in the calcination temperature from 500 to 700 °C, the pore size distribution range of the nanotubes further becomes narrower. When the calcination temperatures were over 700 °C, the peaks of pore size distributions could not be observed. This can be attributed to the formation of rutile phase and sintering and growth of TiO_2 crystallites (Fig. 2 and Table 1). Textural parameters derived from the nitrogen adsorption–desorption isotherm data are summarized in Table 2. When P25 transformed into the titanate nanotubes, there was a significant increase for S_{BET} from 49.3 to 355.7 m^2/g and for pore volume from 0.092 to 1.54 cm^3/g due to the formation of nanotube structures. With increasing calcination temperature, the S_{BET} and pore volumes steadily decreased. At 600 °C, the S_{BET} and pore volume of the nanotubes decreased to 64.3 m^2/g and 0.34 cm^3/g, respectively. This was due to the collapse of the tube structure and the growth of TiO_2 crystallites (Table 1). However, it should be noted that all the TiO_2 products obtained at calcination temperatures lower

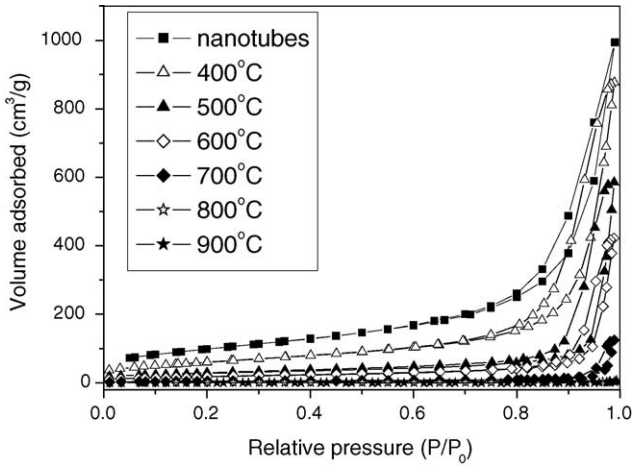

Fig. 3. Nitrogen adsorption–desorption isotherms of the titanate nanotubes calcined at various temperatures.

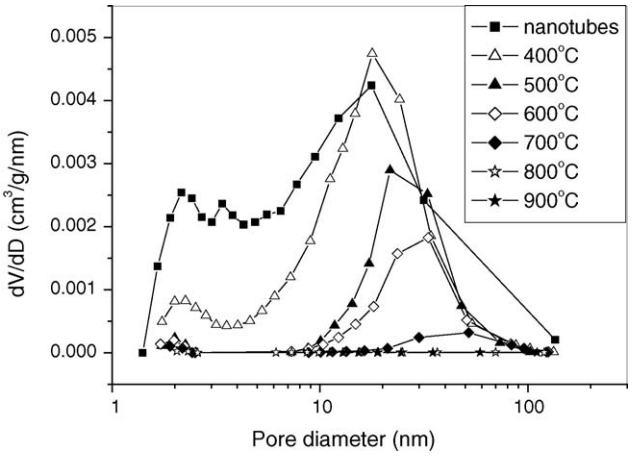

Fig. 4. Pore size distributions of the titanate nanotubes calcined at various temperatures.

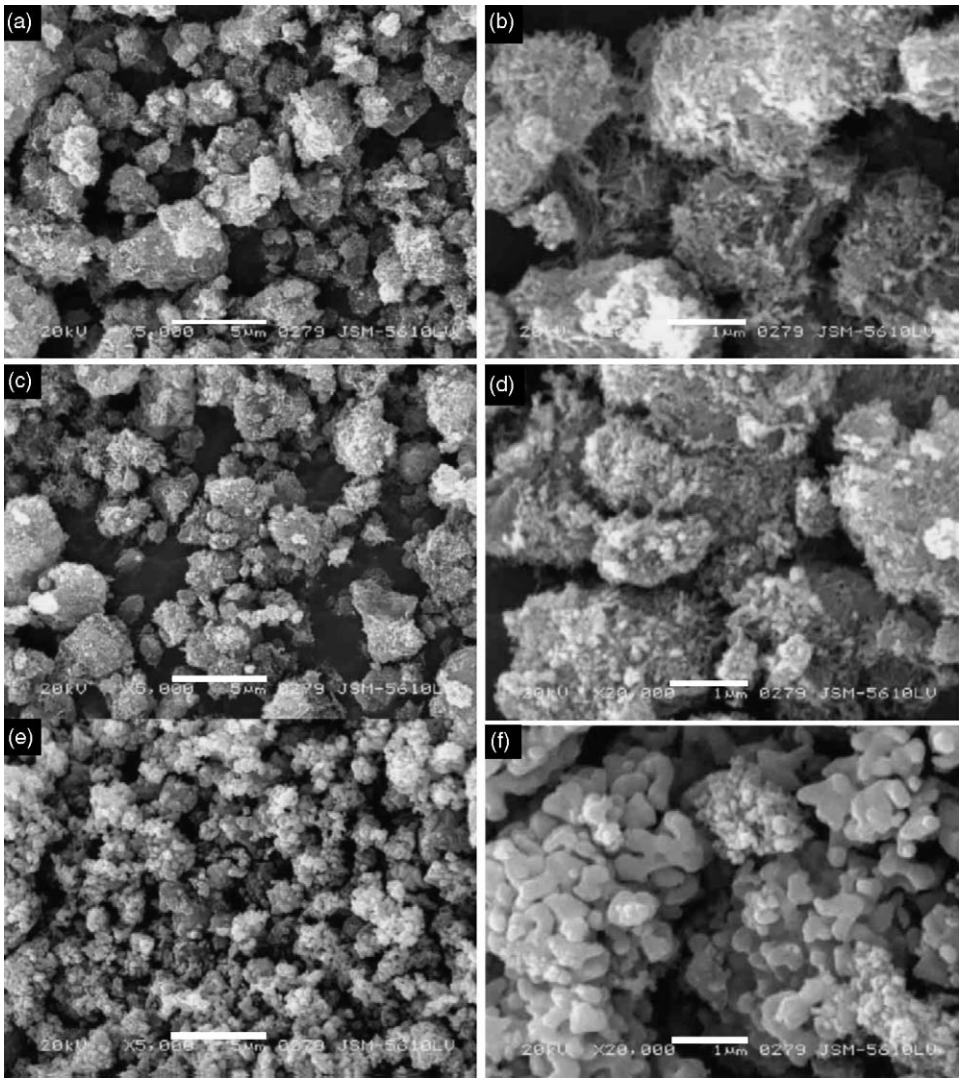

Fig. 5. SEM images of the titanate nanotubes calcined at 400 °C (a and b), 600 °C (c and d), and 700 °C (e and f).

than 700 °C exhibited a higher S_{BET} and pore volume than that of the precursor P25. Especially, at 400 °C and 500 °C, the corresponding S_{BET} of the obtained samples was higher than that of P25 by a factor of about 4.4 and 2.0 times, respectively; while the pore volume was greater than that of P25 by a factor of about 11.0 and 5.6 times, respectively. This indicated that compared with the P25 powders, the advantage of high specific surface area and pore volume of the obtained nanotubes could be preserved, which was beneficial to the enhancement of photocatalytic activity. Further observation from Table 2 indicated that the average pore size of the samples increased from 18.1 to 31.5 nm with increasing calcination temperature (400–600 °C). According to the above facts, there were two factors resulting in the increase of average pore size. One was that the smaller pores inside the nanotubes endured greater stress than the bigger pores formed by the aggregates of nanotubes, so the tube structure collapsed firstly during calcination (Fig. 4) [29]. The other was that the growth of TiO_2 crystallites could result in the formation of bigger pores (Table 1) [29]. At 700 °C, there was an obvious decrease in the S_{BET} and pore volumes due to the phase transition from anatase to rutile, and its values reached 16.1 m^2/g and 0.06 m^3/g, respectively. With further increase in the calcination temperature (700–900 °C), the calcined nanotubes showed a further decrease in S_{BET} and pore volumes. This can be attributed to the formation of rutile and sintering and growth of TiO_2 crystallites.

Table 2
Effects of calcination temperature on the BET specific surface area (S_{BET}) and pore parameters of titanate nanotubes

Samples	S_{BET} (m^2/g)	Pore volume (cm^3/g)	Pore size (nm)
Nanotubes	355.7	1.545	17.3
400	219.2	0.992	18.1
500	99.2	0.503	20.3
600	64.3	0.347	31.5
700	16.1	0.066	44.8
800	3.29	0.007	8.2
900	0.64	0.002	7.2
P25	49.3	0.092	8.3

Fig. 5 shows SEM images of the titanate nanotubes calcined at 400 (a and b), 600 (c and d), and 700 °C (e and f). It can be

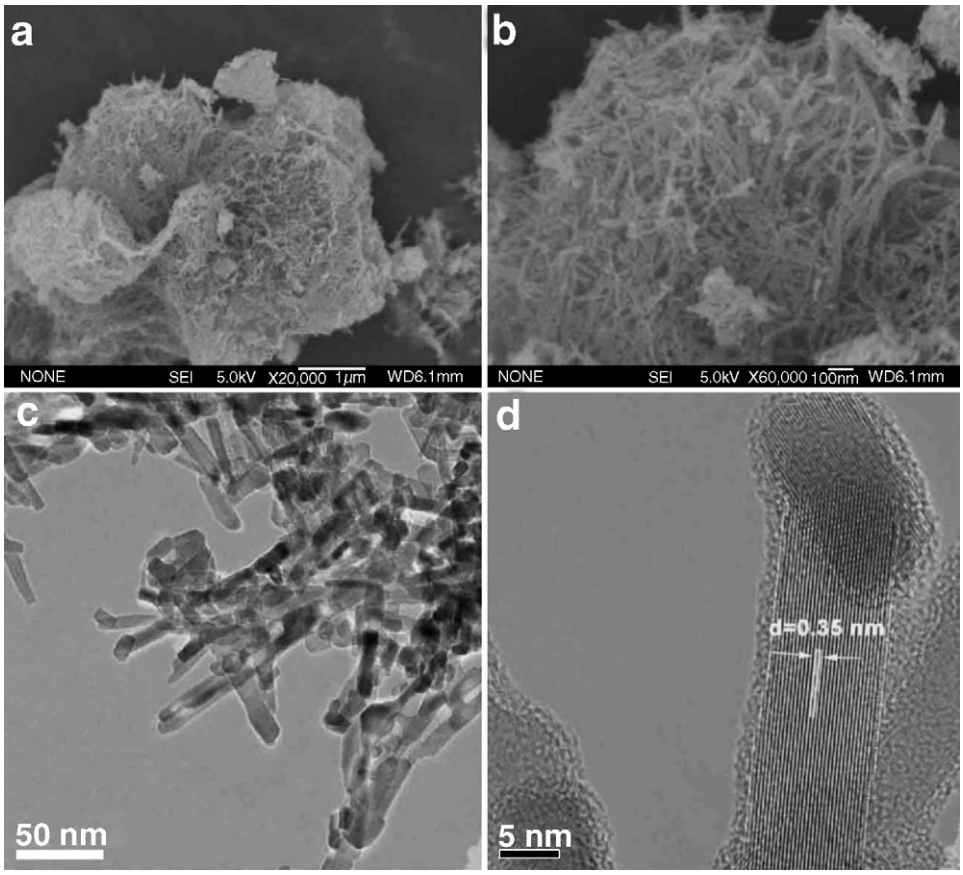

Fig. 6. FESEM images (a and b) and TEM (c) and HRTEM images (d) of the titanate nanotubes calcined at 500 °C.

seen that the surface morphologies of the calcined nanotubes are obviously different at different calcination temperatures. At 400 °C, the calcined nanotubes consisted of TiO_2 particles with a wide particle size distribution from several hundreds of nanometers to several micrometers. Further observation indicated that the TiO_2 particles were porous and were the aggregates of many TiO_2 nanofibers with a diameter of 8–15 nm, resulting in a large S_{BET} and high pore volume (Table 2). When the calcination temperature was increased to 600 °C, the surface morphology of the calcined nanotubes retained a porous structure similar to that of the sample calcined at 400 °C, as shown in Fig. 5c and d. However, the amount of fiber-shaped TiO_2 particles obviously decreased due to a higher calcination temperature. At 700 °C, the surface morphology of the calcined nanotubes had an obvious change. The porous structure and fiber-shaped morphology were difficult to be observed and the calcined nanotubes were some aggregates of dense TiO_2 particles with diameters of 100–300 nm. This can be attributed to the phase transformation of anatase to rutile, resulting in an obvious growth of TiO_2 crystallites (Table 1).

Further insights into the effect of calcination temperature on the surface morphology and phase structure of the nanotubes can be obtained from FESEM and TEM observations. Fig. 6a and b show the FESEM images of the titanate nanotubes calcined at 500 °C. It can be seen that the nanotubes calcined at 500 °C are composed of many TiO_2 nanofibers with a diameter of 8–15 nm and a length of several hundreds of nm. TEM image (Fig. 6c) indicates that the obtained TiO_2 sample is mainly composed of TiO_2 nanorods with a length of 40–120 nm and a diameter of 8–15 nm, in agreement with the previous results [33,37]. HRTEM images (Fig. 6d) suggest that the obtained TiO_2 nanorods are mainly a single crystalline structure in anatase phase. The inter-planar spacing of the nanorods is calculated to be ca. 0.35 nm, corresponding to the (101) crystal plane of anatase. Moreover, there is a layer of amorphous phase close to the outside surface of well-crystallized TiO_2 nanorods, similar to the results found in the titanate nanorods by Lan et al. [37].

3.3. Photocatalytic activity of the titanate nanotubes after calcination at various temperatures

The photocatalytic activity of the titanate nanotubes after calcination at various temperatures was evaluated by photocatalytic oxidation of acetone in air. Fig. 7 shows the relationship between the apparent rate constants (k) of acetone degradation and calcination temperatures. For comparison, the photocatalytic activity of commercial photocatalyst P25 was also tested under identical conditions. Prior to calcination, the nanotubes showed no photocatalytic activity, in contrast to the results reported by Zhu et al. [38]. It was found that the as-prepared hydrogen titanates exhibited decent photocatalytic activity for the photocatalytic oxidation of sulforhodamine (SRB) [38]. The difference in pho-

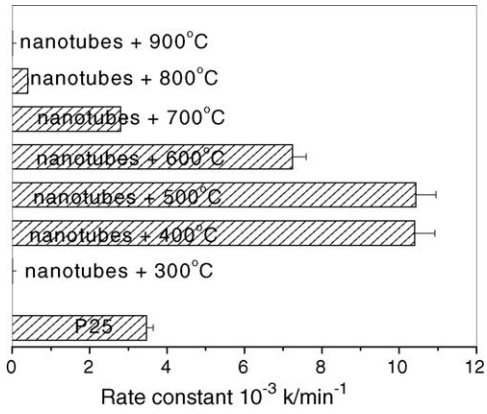

Fig. 7. The dependence of apparent rate constants (k) of the titanate nanotubes on the calcination temperature.

tocatalytic activity of the hydrogen titanates may be attributed to the different experimental conditions. When the calcination temperature was below 400 °C, the calcined samples also showed no photocatalytic activity. This can be due to the absence or low crystallization of anatase phase in the calcined nanotube samples [39–41].

With increasing calcination temperature, the photocatalytic activity of the calcined nanotube samples increased. When the calcination temperature was kept at 400 or 500 °C, the calcined nanotubes showed a very high photocatalytic activity and the corresponding value (k) reached ca. 10.4×10^{-3}, which exceeded that of P25 by a factor of about 3.0 times (Fig. 7). The k was determined to be 3.47×10^{-3} for Degussa P25, which is well known to have good photocatalytic activity. The superior activity of the nanotube samples calcined at 400 and 500 °C can be ascribed to their higher S_{BET} and pore volume (Table 2). Larger specific surface area allows more gaseous reactants to be absorbed onto the surface of the photocatalyst, while higher pore volume results in a rapider diffusion of various gaseous products during the photocatalytic reaction. All these factors contributed to an enhancing photocatalytic activity. However, it should be noted that the factors resulting in the high photoactivity were different in the nanotube samples calcined at 400 and 500 °C. Compared with the nanotube sample calcined at 400 °C, the sample calcined at 500 °C showed a better crystallization in anatase phase (Fig. 2). Therefore, the high photocatalytic activity was kept for the sample calcined at 500 °C though the S_{BET} and pore volume decrease significantly. At 600 °C, the sample also showed a better photocatalytic activity (7.24×10^{-3}) than P25 powder. This can also be attributed to the fact that the former has a higher S_{BET} (64.3 m^2/g) and pore volume (0.34 cm^3/g).

With further increase in the calcination temperature, the photocatalytic activity of the calcined samples decreased. At 700 °C, the k decreased to 2.81×10^{-3}, which was lower than that of P25. When the calcination temperature was above 700 °C, the photocatalytic activity of the TiO_2 samples further decreased. At 900 °C, the photocatalytic activity was difficult to be detected in this study. This could be attributed to the formation of rutile phase, the sintering and growth of TiO_2 crystallites and the decrease of specific surface area and pore volume.

4. Conclusions

The effects of calcination temperature on the microstructures and photocatalytic activity of the titanate nanotubes were investigated and discussed. It was found that the crystalline phase, crystallite size, morphology, specific surface area, pore structures and photocatalytic activity of the titanate nanotubes strongly depended on the calcination temperature. When the calcination temperature was below 400 °C, the calcined samples showed no photocatalytic activity due to the absence or weak crystallization of anatase phase. At 400–600 °C, the photocatalytic activity obviously exceeded that of Degussa P25. Especially, at 400 and 500 °C, the photocatalytic activity of the calcined samples was 3 times higher than that of P25. This could be attributed to the fact that the former had a larger specific surface area and higher pore volume. With further increase in the calcination temperature from 700 to 900 °C, the photocatalytic activity of the calcined samples greatly decreased due to the formation of rutile phase, the sintering and growth of TiO_2 crystallites and the decrease of specific surface area and pore volume.

Acknowledgements

This work was partially supported by the National Natural Science Foundation of China (50272049 and 20473059). This work was also financially supported by the Excellent Young Teachers Program of MOE of China and Project-Sponsored by SRF for ROCS of SEM of China.

References

[1] K. Honda, A. Fujishima, Nature 238 (1972) 37.
[2] M.R. Hoffmann, S.T. Martin, W. Choi, D.W. Bahnemann, Chem. Rev. 95 (1995) 69.
[3] M.A. Fox, M.T. Dulay, Chem. Rev. 93 (1993) 341.
[4] J.C. Zhao, T.X. Wu, K.Q. Wu, K. Oikawa, H. Hidaka, N. Serpone, Environ. Sci. Technol. 32 (1998) 2394.
[5] J.G. Yu, H.G. Yu, B. Cheng, X.J. Zhao, J.C. Yu, W.K. Ho, J. Phys. Chem. B 107 (2003) 13871.
[6] F.B. Li, X.Z. Li, M.F. Hou, Appl. Catal. B 48 (2004) 185.
[7] H.G. Yu, S.C. Lee, C.H. Ao, J.G. Yu, J. Cryst. Growth 280 (2005) 612.
[8] J.G. Yu, X.J. Zhao, Q.N. Zhao, Thin Solid films 379 (2000) 7.
[9] J.G. Yu, J.C. Yu, W.K. Ho, M.K.P. Leung, B. Cheng, G.K. Zhang, X.J. Zhao, Appl. Catal. A 255 (2003) 309.
[10] J. Lin, J.C. Yu, J. Photochem. Photobiol. A 116 (1998) 63.
[11] T. Kasuga, M. Hiramatsu, A. Hoson, T. Sekino, K. Niihara, Langmuir 14 (1998) 3160.
[12] T. Kasuga, M. Hiramatsu, A. Hoson, T. Sekino, K. Niihara, Adv. Mater. 11 (1999) 1307.
[13] Q. Chen, W.Z. Zhou, G.H. Du, L.M. Peng, Adv. Mater. 14 (2002) 1208.
[14] G.H. Du, Q. Chen, R.C. Che, Z.Y. Yuan, L.P. Peng, Appl. Phys. Lett. 79 (2001) 3702.
[15] B.D. Yao, Y.F. Chan, X.Y. Zhang, W.F. Zhang, Z.Y. Yang, N. Wang, Appl. Phys. Lett. 82 (2003) 281.
[16] Z.Y. Yuan, W. Zhou, B.L. Su, Chem. Commun. (2002) 1202.
[17] S.M. Liu, L.M. Gan, L.H. Liu, W.D. Zhang, H.C. Zeng, Chem. Mater. 14 (2002) 1391.
[18] S. Lee, C. Jeon, Y. Park, Chem. Mater. 16 (2004) 4292.
[19] M.S. Sander, M.J. Cote, W. Gu, B.M. Kile, C.P. Tripp, Adv. Mater. 16 (2004) 2052.
[20] A. Thorne, A. Kruth, D. Tunstall, J.T.S. Irvine, W. Zhou, J. Phys. Chem. B 109 (2005) 5439.

[21] D.Y. Zhang, L.M. Qi, Chem. Commun. (2005) 2735.
[22] S.Z. Chu, S. Inoue, K. Wada, D. Li, H. Haneda, S. Awatsu, J. Phys. Chem. B 107 (2003) 6586.
[23] O.K. Varghese, D.W. Gong, M. Paulose, K.G. Ong, E.C. Dickey, C.A. Grimes, Adv. Mater. 15 (2003) 624.
[24] X.M. Sun, Y.D. Li, Chem. Eur. J. 9 (2003) 2229.
[25] K.S.W. Sing, D.H. Everett, R.A.W. Haul, L. Moscou, R.A. Pierotti, J. Rouquerol, T. Siemieniewska, Pure Appl. Chem. 57 (1985) 603.
[26] M.E. Zorn, D.T. Tompkins, W.A. Zeltner, M.A. Anderson, Appl. Catal. B 23 (1999) 1.
[27] J.G. Yu, J.C. Yu, M.K.P. Leung, W.K. Ho, B. Cheng, X.J. Zhao, J.C. Zhao, J. Catal. 217 (2003) 69.
[28] J.C. Yu, J.G. Yu, W.K. Ho, Z.T. Jiang, L.Z. Zhang, Chem. Mater. 14 (2002) 3808.
[29] J.G. Yu, M.H. Zhou, B. Cheng, H.G. Yu, X.J. Zhao, J. Mol. Catal. A 227 (2005) 75.
[30] R. Ma, Y. Bando, T. Sasaki, Chem. Phys. Lett. 380 (2003) 577.
[31] Y. Suzuki, S. Yoshikawa, J. Mater. Res. 19 (2004) 982.
[32] A.R. Armstrong, G. Armstrong, J. Canales, P.G. Bruce, Angew. Chem. Int. Ed. 43 (2004) 2286.
[33] C.C. Tsai, H. Teng, Chem. Mater. 16 (2004) 4352.
[34] M. Wu, G. Lin, D. Chen, G. Wang, D. He, S. Feng, R. Xu, Chem. Mater. 14 (2002) 1974.
[35] J.C. Yu, J.G. Yu, L.Z. Zhang, W.K. Ho, J. Photochem. Photobiol. A 148 (2002) 263.
[36] D.V. Bavykin, V.N. Parmon, A.A. Lapkin, F.C. Walsh, J. Mater. Chem. 14 (2004) 3370.
[37] Y. Lan, X. Gao, H. Zhu, Z. Zheng, T. Yan, F. Wu, S.P. Ringer, D. Song, Adv. Funct. Mater. 15 (2005) 1310.
[38] H. Zhu, X. Gao, Y. Lan, D. Song, Y. Xi, J. Zhao, J. Am. Chem. Soc. 126 (2004) 8380.
[39] J.G. Yu, J.F. Xiong, B. Cheng, S.W. Liu, Appl. Catal. B 60 (2005) 211.
[40] J.G. Yu, J.F. Xiong, B. Cheng, Chin. J. Catal. 26 (2005) 745.
[41] J.G. Yu, H.G. Yu, C.H. Ao, S.C. Lee, J.C. Yu, W.K. Ho, Thin Solid films 496 (2006) 273.